ELSEVIER

Thin Solid Films 316 (1998) 139–147

thin solid films

Effects of antenna wavenumber spectrum and metal end plate on plasma characteristics excited by helicon wave

Shunjiro Shinohara*, Naoya Kaneda, Yoshinobu Kawai

Interdisciplinary Graduate School of Engineering Sciences, Kyushu University, Kasuga, Fukuoka 816-8580, Japan

Abstract

Plasma performance excited by $m = 0$ helicon wave was investigated by the use of an antenna with one, two and four loops, changing the antenna wavenumber spectrum. It was found that the window to obtain a high density plasma, with a density of more than 10^{13} cm^{-3} in the RF power and filling pressure space became narrower when the low wavenumber spectrum part became smaller. However, in the high density region there was no clear relationship between the plasma density and this spectrum and the observed wavelength was determined by the helicon wave dispersion relation. A comparison with an inductively coupled plasma and the effect of the position of a metal end plate on the plasma characteristics are also presented.

Keywords: Helicon wave; Inductively coupled plasma; Wavenumber spectrum; End plate

1. Introduction

The production of high density plasma by a helicon wave [1–18] is becoming more and more important for studies of plasma application and toroidal confinement. However, there are still many problems to be studied, such as the plasma production mechanism [2,3,15,17]. It was shown in previous experiments [9,12] that the helicon wave is only observed after a density jump; a steep density increase to a level of 10^{13} cm^{-3} caused by the application of an RF (radio frequency) power greater than a threshold value.

From the dispersion relation, plasma density increases with an increase in the parallel wavenumber, which means that plasma performance may be affected by the wavenumber spectrum of the antenna used for excitation. Several theoretical attempts have been made to compute the antenna–plasma coupling [19,20] using the given plasma density, but there has been no trial of a self consistent treatment; calculation of the expected plasma density and antenna loading under given external parameters, such as antenna geometry, RF power, RF frequency and filling pressure including plasma transport [6]. The importance of matching the antenna spectrum with the wave damping and/or generation spectrum relating the dispersion relation has been noted [8,21,22], but a detailed study on the antenna spectrum has not been done. Basically, plasma performance can be considered to be partly controlled by the above external parameters. In this article, we investigate plasma characteristics changing the antenna current spectrum over a wide range. In addition, the effect of a metal end plate on the plasma is studied, since boundary conditions are an important influence on the plasma behavior and the data obtained will be very useful for constructing reactor devices.

In this article, after describing the experimental system in Sec. 2 and antenna vacuum field patterns and helicon wave characteristics in Sec. 3, plasma performance is investigated by changing the antenna configurations in order to study the effect of the antenna wavenumber spectrum in Sec. 4. Comparison to the case of an inductively coupled plasma (ICP)

* Corresponding author. Tel.: +81 92 5837649; fax: +81 92 5718894; e-mail: shinoigh@mbox.nc.kyushu-u.ac.jp

0040-6090/98/$19.00
PII S0040-6090(98)00404-0

[23] is also presented. In Sec. 5, the effect of the metal end plate position on plasma performance is studied and finally conclusions are presented in Sec. 6.

2. Experimental set-up

The experimental system is shown in Fig. 1. Argon gas was fed into the Pyrex tube (5 cm in inner diameter) which has an applied magnetic field of 1 kG. The RF power and frequency were < 3 kW and 7 MHz, respectively and the pulse width was 2 ms with a duty of < 0.1. The input power P_{in} was defined as the difference of the incident and reflected power and R (R_v) was total (vacuum) loading resistance. In this experiment, three types of loop antenna, made of copper with 0.3-mm thickness, were wound around the Pyrex tube in order to excite an azimuthal mode number $m = 0$, as shown in Fig. 2: (a) one loop with a width of d; (b) two loops of width d and separated by a distance L; and (c) four loops of width d with a distance L between the two outermost-side loops. For the cases of two and four loops, two types of antenna current directions, i.e. same and alternately opposite current directions, were used. The metal (stainless steel) end plate, 4 cm in diameter with 0.3-mm thickness, was inserted from the left side of the Pyrex tube.

The plasma parameters and excited wave fields were measured by movable Langmuir and magnetic probes inserted into the plasma, respectively. A balanced mixer for the interferometric wave measurements, a boxcar integrator for averaging the data and a 70-GHz microwave interferometer for measurement of the absolute plasma density were also used.

3. Antenna vacuum field pattern and helicon wave characteristics

Excited magnetic fields were measured by a magnetic probe in the absence of the plasma in order to check the antenna field pattern. Fig. 3 shows some examples of the measured and calculated axial profiles of the excited magnetic fields B_z (axial component) for various antenna current configurations; one, two and four loops with same and opposite current directions. The calculation was done under an assumption of a uniform RF current density profile over the antenna width and the calculated value was normalized to match the maximum value of the experimental one. It can be seen from this figure that a very good agreement between calculation and experimental results was found and a uniform current density profile was confirmed even for the case of $d = 10$ cm (not shown). From this, we can easily estimate the external antenna wavenumber spectrum (see Figs. 5, 6, 8 and 11 described later).

In order to ascertain the helicon wave excitation for this type of loop antenna, the dispersion relation and the excited fields were investigated after the density jump. For typical measurements, see Shinohara et al. [9,12] (Shinohara et al. [18]) for the $m = \pm 1$ ($m = 0$) case excited by the helical (spiral) antenna. The relationship between the electron plasma angular frequency ω_{pe} and parallel wavenumber k_z and radial profiles of three components of the excited magnetic fields, an example of which is shown in Fig. 4, agreed well with those calculated from the formulae of $m = 0$ mode [2,7] using the measured radial density profile.

4. Effect of antenna wavenumber spectrum

4.1. One loop case

The antenna width d was varied in order to see the change of plasma performance after the density jump for the one-loop case. Fig. 5a shows the expected

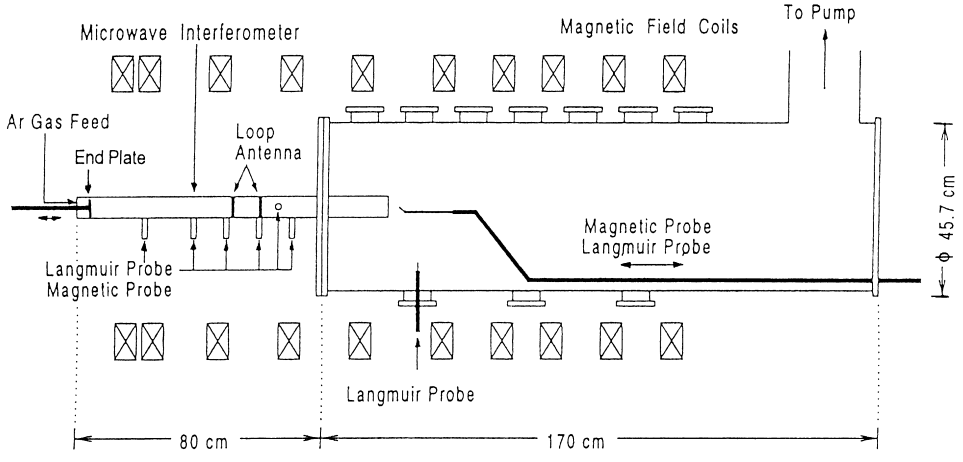

Fig. 1. Schematic view of experimental set-up.

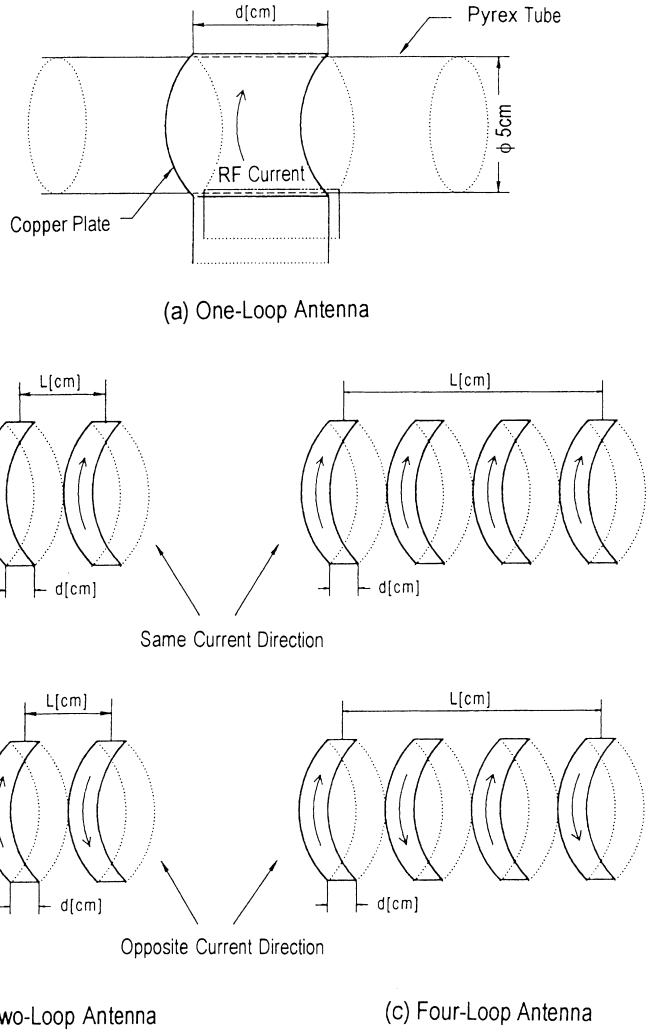

Fig. 2. Antenna structures using: (a) one loop, (b) two loops and (c) four loops.

power spectra of the antenna wavenumber $j(k_z)^2$, where we define $j(k_z)$ as the Fourier spectrum of the antenna current. The maximum values are normalized to be unity for all cases under various antenna configurations described hereafter and antenna–plasma coupling power can be considered to depend on the power spectra. These spectra in Fig. 5a become maximum at $k_z = 0$ and a portion of the radiation power in the higher wavenumber region becomes smaller with the increase in d. From this figure and the typical experimentally obtained value of k_z after the density jump, lying between 0.1 and 0.3 cm^{-1}, it is expected that the antenna–plasma coupling increases with the increase in d from 2 to 10 cm. This may result in a density increase with the constant RF power. Contrary to this expectation, the obtained plasma density n_e (and coupling) after the density jump had little dependence on this antenna width d of 2, 5 and 10 cm, as shown in Fig. 5b: n_e was within the range of $(2.4–2.9) \times 10^{13}$ cm^{-3}. Here, n_e was measured near the antenna region, where the variation of n_e along the axial direction was small (see Fig. 13 for example).

As can be well understood, the excited wave amplitude is derived by integrating the product [16] of the antenna spectrum and the inverse of the dispersion relation $D(k, \omega)$ over the wavenumber k (ω: excited angular frequency). Although one might expect that the dominant k_z would be determined by d with a fixed perpendicular wavenumber, it is free to assume its natural k_z once the wave left the antenna region. In other words, k_z excited in the plasma is determined by the helicon wave dispersion relation (plasma density set by the transport as a parameter), which was confirmed experimentally. Except for the antenna region within an axial length of approximately 10 cm where a standing wave, whose pattern is characterized by the antenna structures, was observed, a propagating wave in both outward directions along the axis was found (see, for example, Fig. 14). This

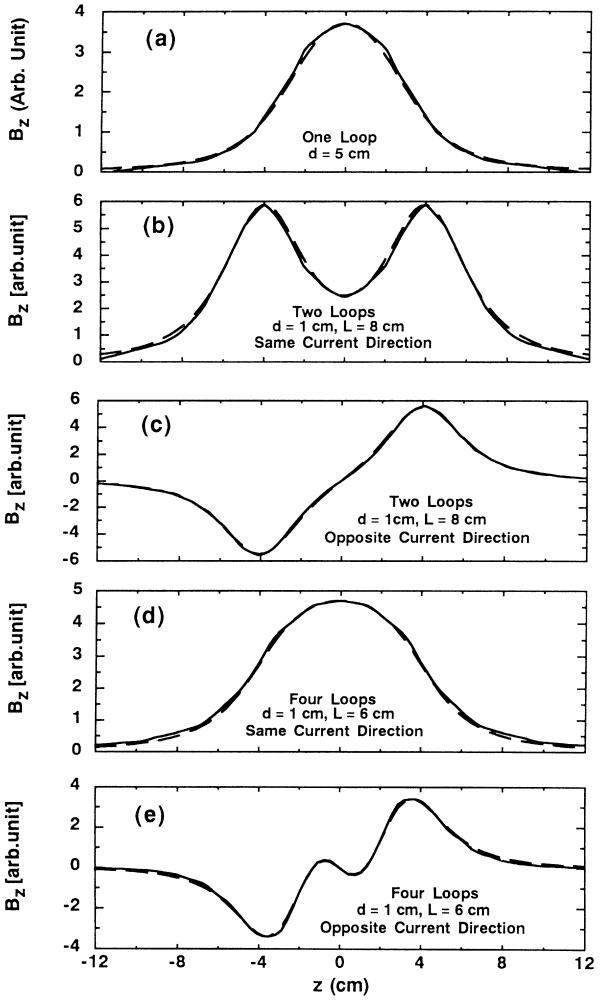

Fig. 3. Axial profiles of excited magnetic fields B_z in the vacuum using: (a) one loop ($d = 5$ cm), two loops ($d = 1$ cm and $L = 8$ cm) with (b) same and (c) opposite current directions, four loops ($d = 1$ cm and $L = 6$ cm) with (d) same and (e) alternately opposite current directions. Here, solid and broken lines show measurement and calculation, respectively and $z = 0$ is defined as the central position of the loops.

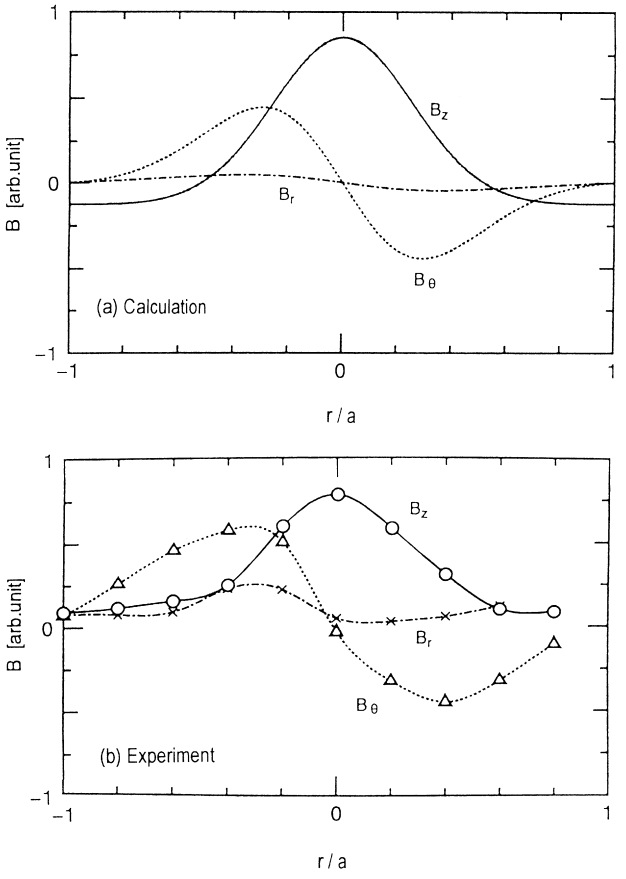

Fig. 4. Radial profiles of the three components of excited magnetic fields, B_r, B_θ and B_z in cylindrical geometry: (a) calculation from measured radial density profile with $m = 0$ mode and (b) measurement by the use of two-loop antenna ($d = 1$ cm and $L = 2$ cm) with same current directions ($P = 11$ mtorr and $P_{in} \sim 1.2$ kW).

feature is the same as for the $m = \pm 1$ excitation case [9,12] and the above discussion may also hold for all cases described later.

4.2. Two loops case

Firstly, the case with the antenna currents in the same directions is described. Figs. 6 and 7a show the $j^2(k_z)$ spectra (similar to Fig. 4a for the one-loop case) and the dependence of n_e on filling pressure P after the density jump, respectively. The distance L was changed while keeping d constant at $d = 1$ cm. Here, for comparison, experimental results for the case without a magnetic field (ICP) are shown in Fig. 7b. In the presence of the magnetic field, n_e rose with the increase in P from approximately 1 to several mtorr and there was a small difference between the different L cases. Note that at $P = 10$ mtorr, the ionization ratio is approximately 10%. In the absence of the magnetic field (Fig. 7b), n_e was lower by close to one order of magnitude compared with the case with the magnetic field (Fig. 7a) and the plasma could not be initiated in the lower filling pressure region. In accordance with the increase in n_e with P, the total resistance R increased gradually regardless of L from ~ 1 (1) Ω to ~ 2.5 (1.5) Ω with (without) the magnetic field. The vacuum resistance R_v was ~ 0.35 Ω.

Next, the case with the antenna current in the opposite directions is described. The $j(k_z)^2$ spectra in Fig. 8 show that the radiation power was zero at $k_z = 0$ and the value of k_z at the first peak position decreased with the increase in L. Again, d was constant at $d = 1$ cm. The dispersion relation of the helicon wave shows that n_e increased with an increase in k_z; in the present case $k_z = 0.1$ cm^{-1} and 0.3 cm^{-1} corresponded to $n_e \sim 1.5 \times 10^{13}$ cm^{-3} and $\sim 5 \times 10^{13}$ cm^{-3}, respectively. Also, the maximum Landau damping rate shows that the phase velocity must be comparable to the thermal electron velocity [2]; $k_z = 0.1$

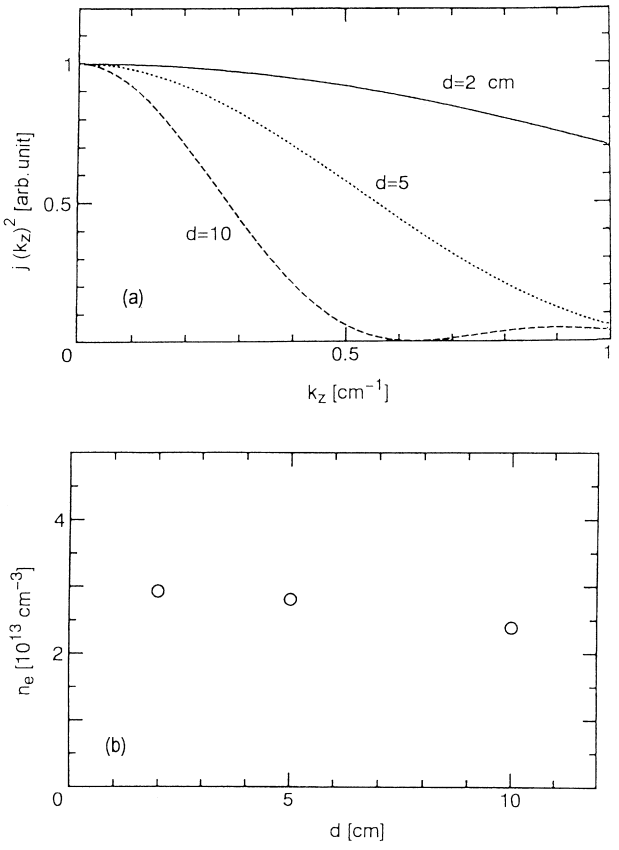

Fig. 5. (a) Power spectra of antenna wavenumber $j(k_z)^2$ and (b) electron density n_e as a function of d for $P = 6.3$ mtorr and $P_{in} \sim 1.3$ kW for the one-loop antenna.

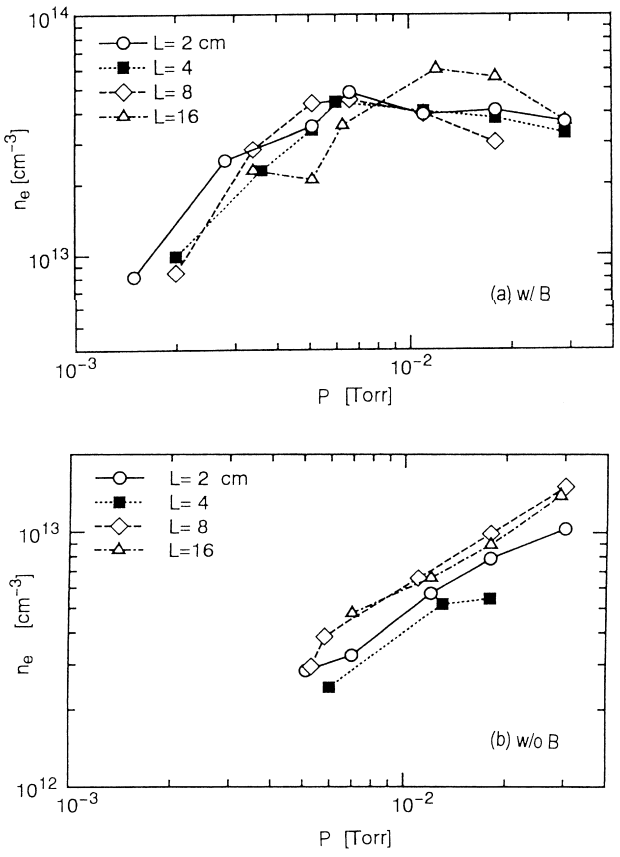

Fig. 7. Electron density n_e as a function of filling pressure P, changing L with a constant d of 1 cm and $P_{in} \sim 1.5$ kW for the two-loop antenna (same current directions). Here, cases (a) and (b) are taken in the presence and absence of the magnetic fields, respectively.

cm^{-1} and 0.3 cm^{-1} correspond to an electron temperature $T_e \sim 37$ eV and ~ 4 eV, respectively. Considering this, a longer L (corresponding to the low wavenumber spectrum part becoming larger) is favorable in obtaining a high density plasma through the initial low density. As expected, the high density plasma could be easily obtained for a wider range of the filling pressure for the longer L case, as shown in Fig. 9a. For the shorter L case, a high density plasma ($n_e > 10^{13}$ cm^{-3}) after the density jump (from low density of an order of 10^{11} cm^{-3}) was obtained in the higher pressure region only ($P > 10$ mtorr). Note that

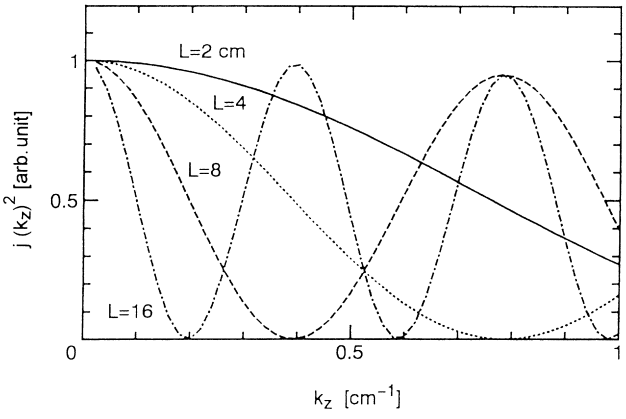

Fig. 6. Power spectra of antenna wavenumber $j(k_z)^2$ for various L values for $d = 1$ cm for the two-loop antenna (same current directions).

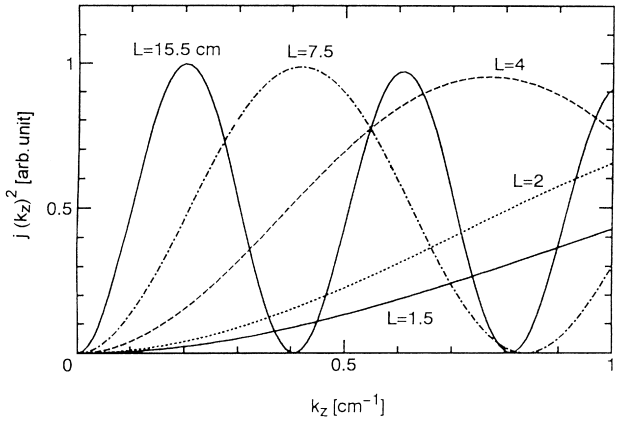

Fig. 8. Power spectra of antenna wavenumber $j(k_z)^2$ for various L values with a constant d of 1 cm for the two-loop antenna (opposite current directions).

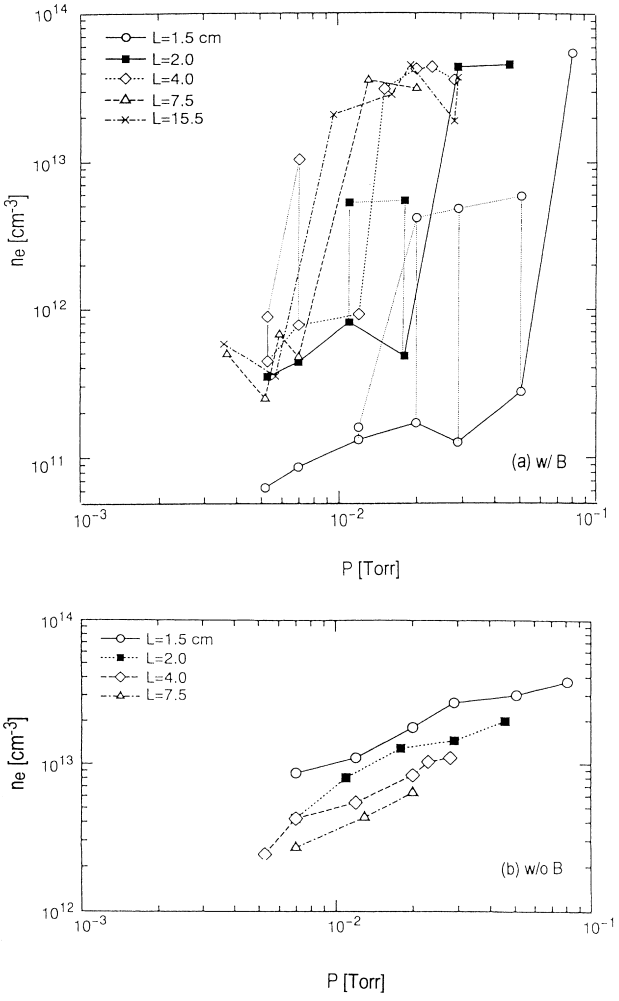

Fig. 9. Electron density n_e as a function of filling pressure P, changing L with a constant d of 1 cm and $P_{in} \sim 1.5$ kW for the two-loop antenna (opposite current directions). Here, cases (a) and (b) are in the presence and absence of the magnetic fields, respectively.

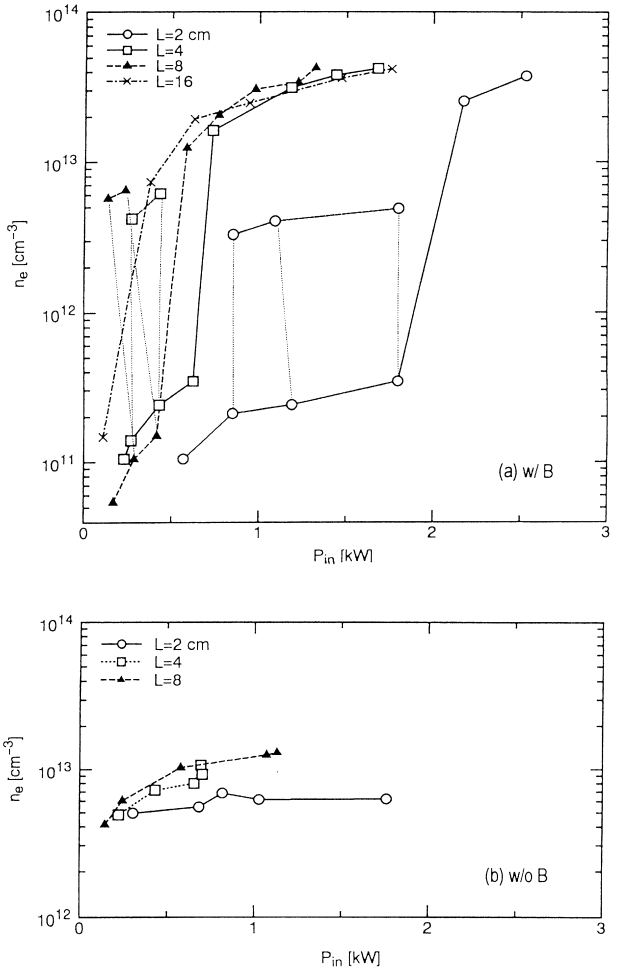

Fig. 10. Relationship between electron density n_e and input power P_{in}, changing L with a constant d of 1 cm and $P = 34$ mtorr for the two-loop antenna (opposite current direction). Here cases (a) and (b) are in the presence and absence of the magnetic fields, respectively.

the initial low density plasma was produced near the antenna and then the density increased with time expanding the high density plasma region (nearly steady-state plasma was obtained after a time of $t >$ 0.6 ms).

This L dependence can also be seen in Fig. 10a. The dependence of n_e on the input power P_{in}, shows that high density could only be obtained with the larger P_{in} for the shorter L case. However, above the threshold values of the RF power and filling pressure (i.e. after the density jump), n_e did not change appreciably regardless of L, P, P_{in} and the antenna configurations (see Figs. 7, 9a and 10a), even though the low density regions were different. Here, R increased abruptly from ~ 0.5 to ~ 1.5 Ω at the density jump with the magnetic field, while without this field R did not increase appreciably with P_{in} and P.

In the intermediate pressure region, which is slightly smaller than the transition value at which the density jump occurs, n_e was unstable and oscillated between low density (low antenna loading) and medium one (middle loading), as shown in Fig. 9a (see vertical dotted lines). Fig. 10a also shows the same phenomena, but the dotted lines are not exactly vertical, since P_{in} decreased due to the change of the RF power reflection coefficient (i.e. the change of the antenna–plasma coupling, which is connected with n_e). Here, n_e oscillated with a frequency on the order of kHz. This medium density (i.e. higher density side) is comparable to that of the ICP cases (Figs. 9b and 10b) where n_e without the magnetic field increased gradually with P and P_{in}.

4.3. Four loops case

Here, the cases of the four-loop antenna, with the antenna currents in the same and alternately opposite

current directions are described. The $j(k_z)^2$ spectra for both cases are shown in Fig. 11, which shows a more peaked profile than those for the one loop (Fig. 5a) and two loops case (Figs. 6 and 8). Fig. 12 shows the dependence of n_e on P for different L values and the results have the same features as the two loops cases. For the case of the same current directions, the density jump was easily obtained, while for the case of the opposite current directions high density plasma could be established only in the higher filling pressure region, which is more apparent for the shorter distance L.

5. Effect of position of metal end plate

In this section, we present the effect of the position of the metal end plate on plasma performance excited by one single loop located on $z = -5$ cm, which is from the left surface of the main chamber. Fig. 13 shows that the ion saturation current I_{is} increased near the antenna region when the metal end plate was approaching the antenna (i.e. from $z = -60$ to -40 cm and -26 cm) and then it decreased as this plate came closer to the antenna ($z = -16$ and -11 cm). If we take T_e as several eV, $I_{is} = 1$ in this figure corresponds to $\sim 5 \times 10^{13}$ cm^{-3}. In accordance with the density change, the excited wavenumber outside the antenna region first became higher and then lower with the smaller amplitude of the wave when the plate approached the antenna, as shown in Fig. 14. This excited wave had a standing wave character near the antenna region (within a half wavelength), which did not change appreciably regardless of the plate position and had a propagating wave outside this region (both to the right and left), which satisfied the dispersion relation of the helicon wave.

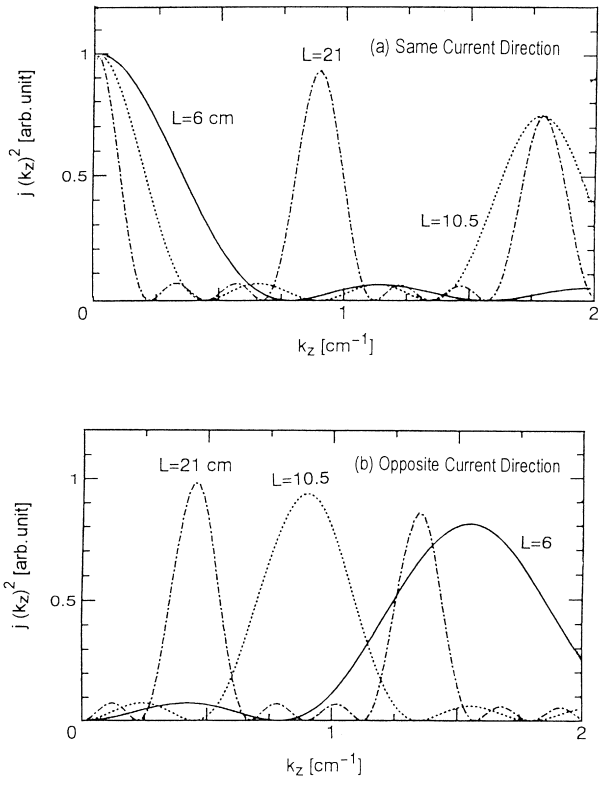

Fig. 11. Power spectra of antenna wavenumber $j(k_z)^2$ for various L values with a constant d of 1 cm. Here, cases (a) and (b) have four current loops with same and alternately opposite directions, respectively.

6. Conclusions

Plasma performance excited by $m = 0$ helicon wave was investigated by the use of the antennae with one, two and four loops, which had the effect of changing the external antenna wavenumber spectrum. It was found that the window to get the high density plasma

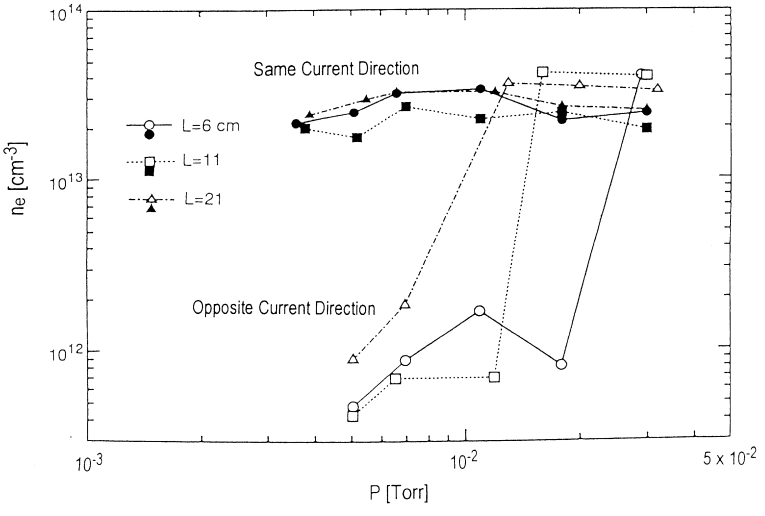

Fig. 12. Dependences of electron density n_e on filling pressure P for various L values with a constant d of 1 cm and $P_{in} \sim 1.5$ kW. Here, closed (open) symbols show four same (alternately opposite) current direction loops.

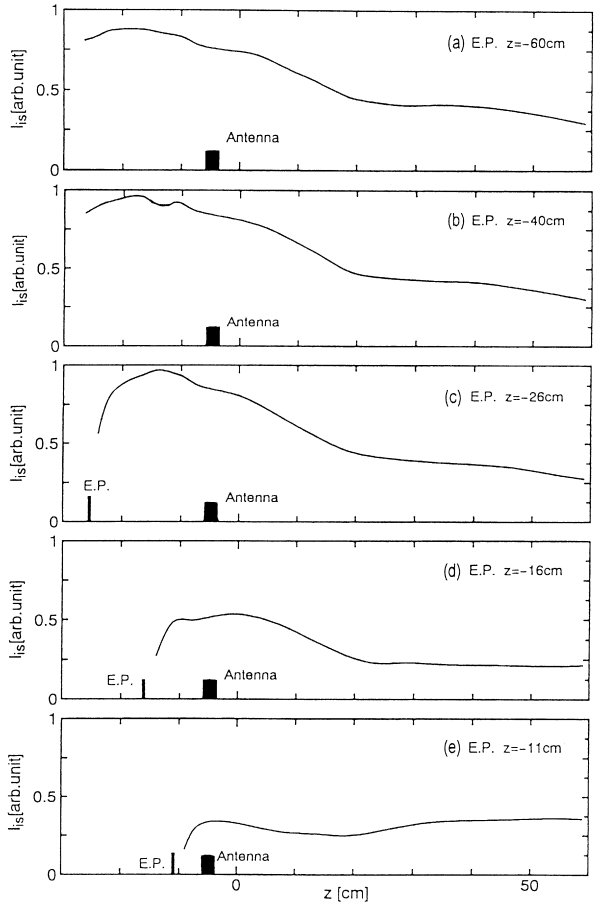

Fig. 13. Axial profiles of ion saturation current I_{is}, when the metal end position (E.P.) was changed. In this case, $d = 2$ cm, $P = 12$ mtorr and $P_{in} \sim 1.5$ kW for the one-loop antenna.

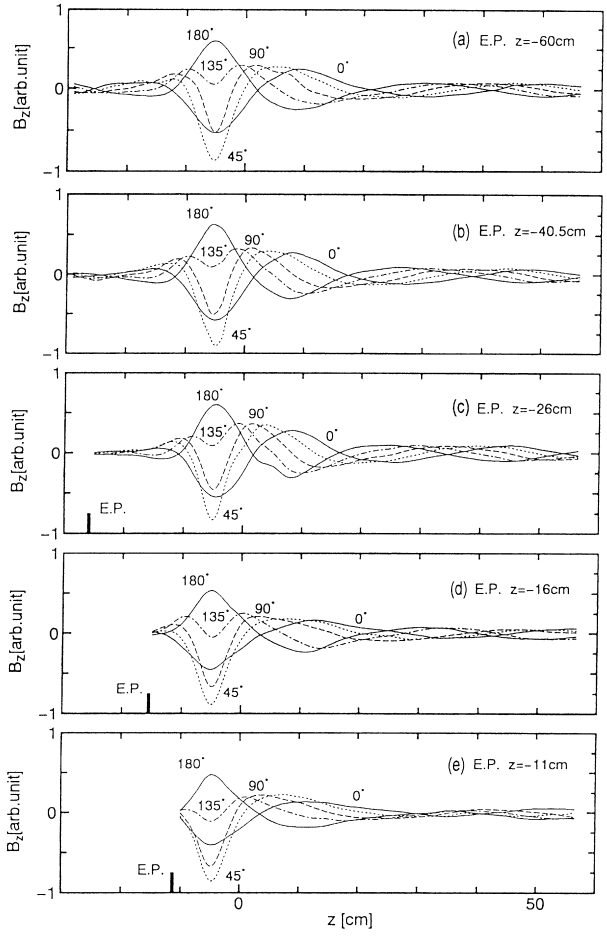

Fig. 14. Axial profiles of excited magnetic fields B_z, when the metal end position (E.P.) was changed under the same conditions as those in Fig. 13.

in the RF power and pressure space became narrower when the low wavenumber part of the spectrum became smaller. However, after the density jump, there was no clear relationship between the plasma density and the external spectrum and the observed wavelength was determined by the helicon wave dispersion relation. For the ICP case, the plasma density and antenna loading were between those for the low and high density regions (i.e. before and after the density jumps) in the presence of the magnetic field.

When the metal end plate came close to the antenna, I_{is} near the antenna and the excited k_z outside the antenna regions first became larger and then smaller when the plate was even closer to the antenna. The excited wave had a standing wave character near the antenna region and had a propagating one outside the region, satisfying the helicon wave dispersion.

Acknowledgements

We thank Dr. Mark Douglas Bowden for checking the English.

References

[1] R.W. Boswell, Plasma Phys. Control. Fusion 26 (1984) 1147.
[2] F.F. Chen, Plasma Phys. Control. Fusion 33 (1991) 339.
[3] A. Komori, T. Shoji, K. Miyamoto, J. Kawai, Y. Kawai, Phys. Fluids B 3 (1991) 893.
[4] P.K. Loewenhardt, B.D. Blackwell, R.W. Boswell, G.D. Conway, S.M. Hamberger, Phys. Rev. Lett. 67 (1991) 2792.
[5] T. Shoji, Y. Sakawa, S. Nakazawa, K. Kadota, T. Sato, Plasma Sources Sci. Technol. 2 (1993) 5.
[6] Y. Yasaka, Y. Hara, Jpn. J. Appl. Phys. 33 (1994) 5950.
[7] F.F. Chen, M.J. Hsieh, M. Light, Plasma Sources Sci. Technol. 3 (1994) 49.
[8] N. Jiwari, T. Fukasawa, H. Kawakami, H. Shindo, Y. Horiike, J. Vac. Sci. Technol. A 12 (1994) 1322.
[9] S. Shinohara, Y. Miyauchi, Y. Kawai, Plasma Phys. Control. Fusion 37 (1995) 1015.
[10] S. Shinohara, Y. Kawai, Jpn. J. Appl. Phys. 34 (1995) L1571.
[11] M. Light, I.D. Sudit, F.F. Chen, D. Arnush, Phys. Plasmas 2 (1995) 4094.
[12] S. Shinohara, Y. Miyauchi, Y. Kawai, Jpn. J. Appl. Phys. 35 (1996) L731.
[13] K. Suzuki, K. Nakamura, H. Sugai, Jpn. J. Appl. Phys. 35 (1996) 4044.
[14] S. Shinohara, S. Takechi, Y. Kawai, Jpn. J. Appl. Phys. 35 (1996) 4503.

[15] F.F. Chen, Phys. Plasmas 3 (1996) 1783, and references therein.
[16] A.R. Ellingboe, R.W. Boswell, Phys. Plasmas 3 (1996) 2797.
[17] S. Shinohara, Jpn. J. Appl. Phys. 36 (1997) 4695, and references therein.
[18] S. Shinohara, S. Takechi, N. Kaneda, Y. Kawai, Plasma Phys. Control. Fusion 39 (1997) 1479.
[19] B. Fischer, M. Krämer, Th. Enk, Plasma Phys. Control. Fusion 36 (1994) 2003.
[20] I.V. Kamenski, G.G. Borg, Phys. Plasmas 3 (1996) 4396.
[21] H. Takeno, Y. Yasaka, O. Sakai, R. Itatani, Nucl. Fusion 35 (1995) 75.
[22] S. Shinohara, Paper presented at 3rd International Conference on Reactive Plasmas and 14th Symposium on Plasma Processing, Nara, 1997, p. 371.
[23] J. Hopwood, Plasma Sources Sci. Technol. 1 (1992) 109, and references therein.